Chapter 4
Pattern Formation by Traveling Localized Modes in Two-Dimensional Dissipative Media with Lattice Potentials

Valentin Besse, Hervé Leblond, Dumitru Mihalache and Boris A. Malomed

Abstract We analyze pattern-formation scenarios in the two-dimensional (2D) complex Ginzburg-Landau (GL) equation with the cubic-quintic nonlinearity and a cellular potential. The equation models laser cavities with built-in gratings, which stabilize 2D patterns. The pattern-building process is initiated by kicking a compound mode, in the form of a dipole, quadrupole, or vortex which is composed of four local peaks. The hopping motion of the kicked mode through the cellular structure leads to the generation of various extended patterns pinned by the structure. In the ring-shaped system, the persisting freely moving dipole hits the stationary pattern from the opposite side, giving rise to several dynamical regimes, including periodic elastic collisions, i.e., persistent cycles of elastic collisions between the moving and quiescent dissipative solitons, and transient regimes featuring several collisions which end up by absorption of one soliton by the other. Another noteworthy result is transformation of a strongly kicked unstable vortex into a stably moving four-peaked cluster.

V. Besse (✉) · H. Leblond · D. Mihalache
LUNAM Université, Université d'Angers, Laboratoire de Photonique d'Angers,
EA 4464,
2 Boulevard Lavoisier, 49000 Angers, France
e-mail: valentin.besse@hotmail.fr

H. Leblond
e-mail: herve.leblond@univ-angers.fr

D. Mihalache
Horia Hulubei National Institute for Physics and Nuclear Engineering, 30 Reactorului,
077125 Magurele-Bucharest, Romania
e-mail: dumitru.mihalache@ifin.nipne.ro

D. Mihalache
Academy of Romanian Scientists, 54 Splaiul Independentei, 050094 Bucharest, Romania

B.A. Malomed
Department of Physical Electronics, Faculty of Engineering, Tel Aviv University,
69978 Tel Aviv, Israel
e-mail: malomed@post.tau.ac.il

J.F.R. Archilla et al. (eds.), *Quodons in Mica*, Springer Series
in Materials Science 221, DOI 10.1007/978-3-319-21045-2_4

4.1 Introduction

4.1.1 Dissipative Solitons: A Brief Overview

Spatial dissipative solitons are self-trapped beams of light [4, 5] or plasmonic waves [17, 28, 31, 35, 46, 49, 52, 53, 66, 67] propagating in planar or bulk waveguides. They result from the balance between diffraction and self-focusing nonlinearity, which is maintained simultaneously with the balance between the material loss and compensating gain. Due to their basic nature, the spatial dissipative solitons are modes of profound significance to nonlinear photonics (optics and plasmonics), as concerns the fundamental studies and potential applications alike. In particular, a straightforward possibility is to use sufficiently narrow spatial-soliton beams as signal carriers in all-optical data-processing schemes. This application, as well as other settings in which the solitons occur, stresses the importance of the stabilization of the dissipative-soliton modes, and of development of enabling techniques for the generation and steering of such planar and bulk beams.

In terms of the theoretical description, basic models producing spatial dissipative solitons dynamics are based on complex Ginzburg-Landau (GL) equations. The prototypical one is the complex GL equation with the cubic nonlinearity, which includes the conservative paraxial-diffraction and Kerr terms, cubic loss with coefficient $\varepsilon > 0$, which represents two-photon absorption in the medium, and the spatially uniform linear gain, with strength $\gamma > 0$, which aims to compensate the loss [79]:

$$\frac{\partial u}{\partial z} = \frac{i}{2}\nabla_{\perp}^{2} u - (\varepsilon - i\beta)\,|u|^{2} u + \delta u. \tag{4.1}$$

Here u is the complex amplitude of the electromagnetic wave in the spatial domain, z is the propagation distance, the paraxial-diffraction operator $\nabla_{\perp}^{2}$ acts on transverse coordinates (x, y) in the case of the propagation in the bulk, or on the single coordinate, x, in the planar waveguide. Accordingly, (4.1) is considered as two- or one-dimensional (2D or 1D) equation in those two cases. The equation is normalized so that the diffraction coefficient is 1, while β is the Kerr coefficient, $\beta > 0$ and $\beta < 0$ corresponding to the self-focusing and self-defocusing signs of the nonlinearity, respectively.

A more general version of the complex GL equation may include an imaginary part of the diffraction coefficient, which is essential, in particular, for the use of the equation as a model of the traveling-wave convection [27, 48]. However, in optical models that coefficient, which would represent diffusivity of photons, is usually absent, as light is not, normally, subject to diffusion.

A well-known fact is that the 1D version of (4.1) gives rise to an exact solution in the form of an exact *chirped* dissipative soliton, which is often called a *Pereira-Stenflo soliton* [79]:

$$u(x,z) = Ae^{ikz}\left[\operatorname{sech}(\kappa x)\right]^{1+i\mu},$$
$$A^2 = 3\delta/(2\varepsilon),\ \kappa^2 = \delta/\mu,\ k = (\delta/2)\left(\mu^{-1} - \mu\right),$$

where the chirp coefficient is

$$\mu = \sqrt{(3\beta/2\varepsilon)^2 + 2} - 3\beta/(2\varepsilon). \tag{4.2}$$

This exact solution is subject to an obvious instability, due to the action of the uniform linear gain on the zero background far from the soliton's core. Therefore, an important problem is the design of physically relevant models which may produce stable spatial dissipative solitons.

One possibility to achieve stabilization of dissipative solitons is provided by systems of linearly coupled complex GL equations, which model dual-core waveguides, with the linear gain and loss acting in different cores [10, 11, 59, 63]. The simplest example of the action of this stabilization mechanism is offered by the following system [11]:

$$\frac{\partial u}{\partial z} = \frac{i}{2}\nabla_\perp^2 u - (\varepsilon - i\beta)|u|^2 u + \delta u + i\lambda v, \tag{4.3}$$
$$\frac{\partial v}{\partial z} = (iq - \Gamma)v + i\lambda u, \tag{4.4}$$

where λ is the linear-coupling coefficient, $v(x,z)$ and $\Gamma > 0$ are the field amplitude and the linear loss strength in the stabilizing dissipative core, and q is a wavenumber mismatch between the cores, if any. In the case of $q = 0$, the zero background is stable in the framework of (4.3) and (4.4) under condition

$$\delta < \Gamma < \lambda^2/\delta. \tag{4.5}$$

The same ansatz (4.2) which produces the Pereira-Stenflo soliton for the single complex GL equation yields an exact solution of system (4.3), (4.4):

$$\{u(x,z), v(x,z)\} = \{A, B\}\, e^{ikz}\left[\operatorname{sech}(\kappa x)\right]^{1+i\mu}, \tag{4.6}$$

where chirp μ given by the same expression (4.2) as above, and

$$B = i\lambda\left[\Gamma + i(k-q)\right]^{-1} A. \tag{4.7}$$

A stable soliton is obtained if a *pair* of distinct solutions are found, compatible with the condition of the stability for the zero background, i.e., (4.5) in the case of $q = 0$. Then, the soliton with the larger amplitude is stable, while the other one, with a smaller amplitude, plays the role of an unstable *separatrix* which delineates the boundary between attraction basins of the stable soliton coexisting the stable zero

solution [11]. In the case of $q = 0$, the condition of the coexistence of two soliton solutions reduces to

$$\delta\Gamma\left(1-\mu^2\right) > 4\mu^2\left[\left(\lambda^2-\delta\Gamma\right)+2\Gamma\left(\Gamma-\delta\right)\right]. \tag{4.8}$$

In particular, it follows from (4.8) and (4.2) that a related necessary condition, $\mu < 1$, implies $\varepsilon < 3\beta$, i.e., the Kerr coefficient, β, must feature the self-focusing sign, and the cubic-loss coefficient, ε, must be sufficiently small in comparison with β.

Getting back to models based on the single complex GL equation, stable solitons can also be generated by the equation with cubic gain "sandwiched" between linear and quintic loss terms, which corresponds to the following generalization of (4.1):

$$\frac{\partial u}{\partial z} = \frac{i}{2}\nabla_\perp^2 u + (\varepsilon + i\beta)|u|^2 u - (\mu + i\nu)|u|^2 u - \delta u, \tag{4.9}$$

with $\varepsilon > 0$, $\mu > 0$, $\delta > 0$, and $\nu \geq 0$. The linear loss, represented by coefficient δ, provides for the stability of the zero solution to (4.9). Originally, the complex GL equation of the cubic-quintic type was introduced [80] as a model for the creation of stable 2D localized modes. Following that work, similar models were derived or proposed as phenomenological ones in various settings. Many 1D and 2D solutions for dissipative solitons have been found in the framework of such equations [2, 3, 6, 21, 23–25, 29, 38, 42, 50, 57, 62, 65, 69–76, 81, 84, 86–90, 92–95, 98].

Another method for creating stable localized modes makes use of linear gain applied at a "hot spot", i.e. a localized amplifying region embedded into a bulk lossy waveguide (recent reviews of this topic can be found in [44, 60]). The experimental technique which allows one to create localized gain by means of strongly inhomogeneous distributions of dopants implanted into the lossy waveguide, which produce the gain if pumped by an external source of light, is well known [41]. Another possibility is even more feasible and versatile: the dopant density may be uniform, while the external pump beam is focused on the location where the hot spot should be created.

Supporting dissipative solitons by the localized gain was first proposed in the framework for a gap soliton pinned to a hot spot in a lossy Bragg grating [56]. The corresponding model is based on the system of coupled-mode equations for counter-propagating waves, $u(x, z)$ and $u(x, z)$, coupled by the Bragg reflection:

$$\begin{aligned} iu_z + iu_x + v + \left(|u|^2 + 2|v|^2\right)u \\ = -i\delta u + i\left(\Gamma_1 + i\Gamma_2\right)\delta(x)u, \\ iv_z - iv_x + u + \left(|v|^2 + 2|u|^2\right)v \\ = -i\delta v + i\left(\Gamma_1 + i\Gamma_2\right)\delta(x)v, \end{aligned}$$

where the tilt of the light beam and the reflection coefficients are normalized to be 1, the nonlinear terms account for the self- and cross-phase modulation induced by

the Kerr effect, $\delta > 0$ is the linear-loss parameter, $\Gamma_1 > 0$ represents the local gain applied at the hot spot, which is approximated by the Dirac's delta-function, $\delta(x)$, and the imaginary part of the gain coefficient, $\Gamma_2 \geq 0$, accounts for a possible attractive potential induced by the hot spot.

The hot spot embedded into the usual planar waveguide is described by the following modification of (4.1):

$$\frac{\partial u}{\partial z} = \frac{i}{2}\nabla_{\perp}^2 u - (\varepsilon - i\beta)\,|u|^2 u - \delta u + (\Gamma_1 + i\Gamma_2)\,\delta(x)u, \tag{4.10}$$

where, as well as in (4.10) and (4.11), $\Gamma_1 > 0$ is assumed, and the $\delta > 0$ represents the linear loss in the bulk waveguide. Another hot-spot model, based on the complex GL equation with the combination of cubic-quintic terms, was introduced in [22]:

$$\frac{\partial u}{\partial z} = \frac{i}{2}\frac{\partial^2 u}{\partial x^2} + i|u|^2 u - i\nu|u|^2 u - \delta u + \Gamma e^{-x^2/w^2}|u|^2 u, \tag{4.11}$$

where $\nu > 0$ represents the quintic self-defocusing term, $\delta > 0$ and $\Gamma > 0$ are, as above, strengths of the bulk losses and localized *cubic* gain, and w is the width of the hot spot (an approximation corresponding to $w \to 0$, with the hot spot in the form of the delta-function, may be applied here too). While solitons in uniform media, supported by the cubic gain, are always unstable against the blowup in the absence of the quintic loss [85], the analysis reported in [22] demonstrates that *stable* dissipative localized modes in the uniform lossy medium may be supported by the *unsaturated* localized cubic gain in the model based on (4.11).

Models combining the localized gain, the uniform Kerr nonlinearity, and the linear loss have been developed in various settings, see recent reviews [44, 60]. In particular, periodic amplifying structures [45, 104], as well as extended patterns [1, 103], have been studied. The numerical analysis has made it also possible to study 2D settings, in which, most notably, stable localized vortices can be supported by the gain confined to an annular-shaped area [19, 20, 40, 54, 86].

In addition to the hot spot, one can naturally define a "warm spot", in the 2D complex GL with the cubic-quintic nonlinearity, where the coefficient of the linear loss is spatially profiled with a minimum at the warm spot ($\mathbf{r} = 0$) [86]. The equation may be taken as the 2D version of (4.9) with

$$\Gamma(r) = \Gamma_0 + \Gamma_2 r^2, \tag{4.12}$$

where r is the radial coordinate, coefficients Γ_0 and Γ_2 being positive. This 2D model gives rise to a great variety of stable modes pinned to the warm spot. Depending on values of parameters in (4.9) and (4.12), they are simple vortices, rotating elliptic, eccentric, and slanted vortices, spinning crescents, etc. [86].

The use of the spatial modulation of loss coefficients opens another way for the stabilization of spatial dissipative solitons: as shown in [18], the solitons may be readily made stable if the spatially uniform linear gain is combined with the local

strength of the cubic loss, $\varepsilon(r)$, growing from the center to periphery at any rate faster than r^D, where r is the distance from the center and D the spatial dimension. This setting is described by the following modification of (4.1):

$$\frac{\partial u}{\partial z} = \frac{i}{2}\nabla_{\perp}^2 u - [\varepsilon(r) - i\beta]\,|u|^2 u + \delta u, \tag{4.13}$$

with $\delta > 0$ and, as said above, $\lim_{r\to\infty}\left[r^D/\varepsilon(r)\right] = 0$, for $D = 1$ or 2.

4.1.2 The Subject of the Consideration in the Present Chapter

The theme of the this chapter are 2D dissipative solitons in models of optical laser cavities [13, 14, 32, 36, 37, 43, 64, 82, 83, 96, 97, 99, 100] and plasmonic microcavities [17, 28, 31, 35, 46, 49, 52, 53, 66, 67], based on complex cubic-quintic GL equations. Conservative terms in these equations represent the diffraction and self-focusing nonlinearity, while dissipative terms account for linear and nonlinear loss and gain terms. Beyond the limits of optics and plasmonic, these complex GL equations belong to the generic class of dissipative pattern-formation models [8, 58], which apply to the description of condensates of bosonic quasi-particles in solid-state media [7, 9, 47, 61], reaction-diffusion systems [26], and superconductivity [39].

An essential ingredient of many laser cavities is a transverse periodic grating, which can be fabricated by means of available technologies [91]. In addition to the permanent gratings, virtual photonic lattices may be induced in photorefractive crystals as interference patterns by pairs of pump beams with the ordinary polarization, which illuminate the crystal along axes x and y, while the probe beam with the extraordinary polarization is launched along z [34]. A 2D cavity model with the grating was introduced in [51]. It is based on the complex GL equation with the cubic-quintic nonlinearity and the cellular (lattice) potential, which represents the grating. In fact, the laser cavity equipped with the grating may be considered as a photonic crystal built in the active medium. Periodic potentials also occur in models of passive optical systems, which are driven by external beams and operate in the temporal domain, unlike the active systems which act in the spatial domain [33, 55].

Localized vortices, alias vortex solitons, constitute an important species of self-trapped modes in 2D settings. In uniform media, dissipative vortex solitons cannot be stable without the presence of a diffusion term [24, 25, 73–76]. However, such a term is absent in models of waveguiding systems (this term may sometimes be relevant in temporal-domain optical models [30]). Nevertheless, compound vortices, built as complexes of four peaks pinned to the lattice potential, may be made stable in models including the grating in the absence of the diffusion [51]. Using this possibility, stable 2D [78] and 3D [77] vortical dissipative solitons have been found in the framework of complex GL equations including trapping potentials.

In a majority of previous works, the studies of various 2D localized patterns have been focused on their stabilization by means of the lattice potentials. Another relevant issue is mobility of 2D dissipative solitons in the presence of the underlying lattice, which is closely related to the general topic of the present volume as a whole, i.e., mobility of localized modes across lattice potentials. Note that dissipative solitons may move without friction only if the diffusion term is absent, therefore the mobility is a relevant issue for the diffusion-free models of laser cavities (as stressed above, the absence of diffusion is an inherent feature of the cavity models). Localized modes can be set in motion by the application of a kick to them, which, in the context of the laser-cavity models, implies launching a tilted beam into the system. Recently, the mobility of kicked 2D fundamental solitons in the complex GL equation with the cubic-quintic nonlinearity and a cellular potential was studied in [15]. It has been demonstrated that the kicked soliton, hopping through the periodic structure, leaves in its wake various patterns in the form of single- or multi-peak states trapped by the periodic potential. In the case of periodic boundary conditions (b.c.), which correspond to an annular system, the free soliton completes the round trip and hits the pattern that it has originally created. Depending on parameters, the free soliton may be absorbed by the pinned mode (immediately, or after several – up to five – cycles of quasi-elastic collisions), or the result may be a regime of periodic elastic collisions, which features periodic cycles of passage of the moving soliton through the quiescent one.

A natural extension of the analysis performed in [15] and other recent works is to study of the mobility of kicked soliton complexes, such as dipoles, quadrupoles, and compound vortices, and various scenarios of the dynamical pattern formation initiated by such moving complex modes, in the framework of the 2D cubic-quintic complex GL equation with the lattice potential. This is the subject of the present Chapter. In fact, such configurations are truly two-dimensional ones, while the dynamical regimes for kicked fundamental solitons, which were earlier studied in [15], actually represent quasi-1D settings.

The chapter is structured as follows. The model is formulated in Sect. 4.2, which is followed by the presentation of systematic numerical results for the pattern formation carried out by moving dipoles, quadrupoles, and vortices of two types (“rhombuses” and “squares”, alias onsite and intersite-centered ones) in Sects. 4.3, 4.4, and 4.5, respectively. The chapter is concluded by Sect. 4.6.

One of essential findings is that the interaction of a freely moving dipole with pinned patterns, originally created by the same kicked dipole, gives rise to new outcomes under the periodic b.c. In particular, the quiescent dipole can be absorbed (“cleared”) by the moving one, which may have obvious applications to the design of all-optical data-processing schemes, where one may need to install or remove a blocking soliton. Also noteworthy is the transformation of an unstable vortex by a strong kick into a stable moving four-soliton cluster. Some additional details concerning these issues can be found in recent publication [16].

4.2 The Cubic-Quintic Complex Ginzburg-Landau Model with the Cellular Potential

The cubic-quintic complex GL equation with a periodic potential is written as

$$\frac{\partial u}{\partial Z} = \left[-\delta + \frac{i}{2}\nabla_{\perp}^2 + (i+\varepsilon)|u|^2 - (i\nu+\mu)|u|^4 + iV(X,Y) \right] u. \tag{4.14}$$

It describes the evolution of the amplitude of electromagnetic field $u(X, Y, Z)$ along propagation direction Z, with transverse Laplacian $\nabla_{\perp}^2 = \frac{\partial^2}{\partial X^2} + \frac{\partial}{\partial Y^2}$. Parameter δ is the linear-loss coefficient, ε is the cubic gain, μ the quintic loss, and ν the quintic self-defocusing coefficient (it accounts for the saturation of the Kerr effect if $\nu > 0$). The 2D periodic potential with amplitude V_0 is taken in the usual form, $V(X, Y) = V_0 [\cos(2X) + \cos(2Y)]$, with the period normalized to be π. The total power of the field is also defined as usual,

$$P = \int \int |u(X,Y)|^2 \, dX dY. \tag{4.15}$$

We solved complex GL equation (4.14) by means of the fourth-order Runge-Kutta algorithm in the Z-direction, and five-point finite-difference scheme for the computation of the transverse Laplacian $\nabla_{\perp}^2$. Periodic boundary conditions (b.c.) were used for the study of kicked dipoles and quadrupoles, and absorbing b.c. for kicked vortices.

Values of coefficients chosen for numerical simulations are $\delta = 0.4$, $\varepsilon = 1.85$, $\mu = 1$, $\nu = 0.1$, and $V_0 = -1$. This choice corresponds to a set of parameters for which the initial static configurations for the dipoles, quadrupoles, and vortices are stable. The kick is applied to then in the usual way, by adding the linear phase profile to the initial field:

$$u_0(X,Y) \to u_0(X,Y) \exp(i\mathbf{k}_0 \cdot \mathbf{r}), \tag{4.16}$$

where $\mathbf{r} \equiv \{X, Y\}$. The key parameters are length k_0 of kick vector $\mathbf{k}_0$, and angle θ which it makes with the X-axis, i.e.,

$$\mathbf{k}_0 = (k_0 \cos\theta, k_0 \sin\theta). \tag{4.17}$$

In the laser setup the kick corresponds to a small deviation of the propagation direction of the beam from the Z axis. If K_0 is the full wave number and φ is the deviation angle, the length of the transverse wave vector in physical units is $K_0 \sin\varphi$, which corresponds to k_0 in the normalized form. Below, we investigate the influence of kick parameters k_0 and θ, defined as per (4.17), on a variety of multi-soliton complexes, which are created by moving dipoles, quadrupoles, or vortices (of both rhombus- and square-types) in the 2D complex GL medium with the cellular potential.

4.3 The Pattern Formation by Kicked Dipoles

In this section we consider the simplest soliton complex in the form of a stable vertical dipole, which consists of a pair of solitons aligned along the Y-axis and mutually locked with phase difference π, which is shown in Fig. 4.1. The issue is mobility of such modes, and formation of new patterns in the wake of moving ones. The results are obtained by means of systematic direct simulations.

4.3.1 Generation of Multi-dipole Patterns by a Dipole Moving in the Transverse Direction

First, the dipole is set in motion by the application of the kick in the horizontal (X) direction (i.e., transversely to the dipole's axis), as per (4.16) and (4.17) with $\theta = 0$.

As shown in Fig. 4.2, the moving dipole multiplies into a set of secondary ones, similar to the outcome of the evolution of the kicked fundamental soliton [15]. Each newly created dipole features the fixed phase shift π between two constituent solitons, and the entire pattern, established as the result of the evolution, is robust. The particular configuration displayed in Fig. 4.2 is a chain of five trapped dipoles, and a free one, which has wrapped up the motion and reappears from the left edge, moving to the right, due to the periodic b.c. Then, the free dipole will hit the pinned chain, and will be absorbed by it, yielding a pattern built of five quiescent dipoles. Immediately after the collision, the pattern features intrinsic oscillations, which are gradually damped.

The snapshot shown in Fig. 4.2 corroborates an inference made from the analysis of numerical results: The largest number of the dipoles generated by the initially

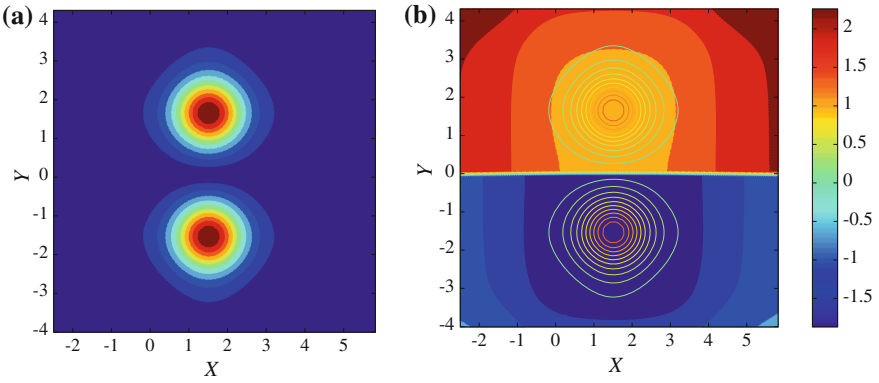

Fig. 4.1 The distribution of the amplitude (**a**) and phase (in units of π) (**b**) in the stable quiescent dipole mode

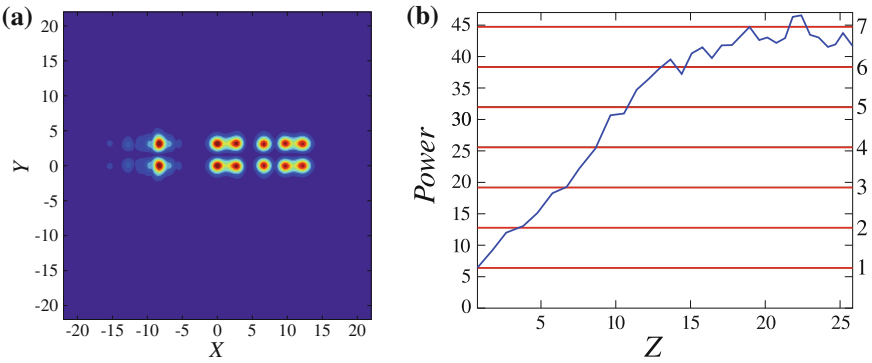

Fig. 4.2 **a** Field $|u(X, Y)|$ produced by the horizontally kicked (with $\theta = 0$) *vertical* dipole at $Z = 22.410$, for $k_0 = 1.665$. In this panel, the leftmost dipole is moving to the *right*. **b** The evolution of the pattern produced by the horizontally kicked dipole, shown in terms of the total power of the field as a function of propagation distance Z. The set of *horizontal red lines* show power levels corresponding to different numbers (n) of quiescent dipoles

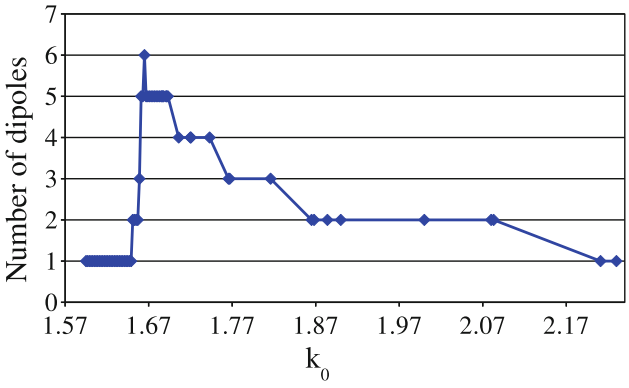

Fig. 4.3 The number of dipoles in the final configuration versus the kick strength, k_0, applied to the vertical dipole in the horizontal direction

kicked one is six, including one moving dipole and five identical quiescent ones. It is worthy to note that, as seen in Fig. 4.2b, in this case the total power (4.15) of the finally established set of six dipoles is close to the net power corresponding to *seven* quiescent ones, which is explained by the observation that the power of the stably moving dipole is, approximately, twice that of its quiescent counterpart.

To study the outcome of this dynamical pattern-formation scenario in a systematic form, we monitored the number of output solitons as a function of the kick's strength, k_0. These results are summarized in Fig. 4.3, which provides an adequate overall characterization of the interactions, including a potential possibility to use these interactions for the design of data-processing setups.

Below the threshold value of the kick's strength, whose numerically found value is

$$k_0^{(\mathrm{thr})}\,(\theta = 0) \approx 1.651, \tag{4.18}$$

the kicked dipole exhibits damped oscillations, remaining trapped near a local minimum of the cellular potential. Then, as seen in Fig. 4.3, the number of dipoles initially increases steeply with k_0 , reaching (as mentioned above) a maximum of six at $k_0 = 1.665$. It is worthy to mention that this value is different from those, ranging in interval $k_0 \in [1.6927, 1.6942]$, in which the maximum number of secondary solitons is reached in the case when the kick is applied to a fundamental soliton [15]. This observation suggests that building the structures by the kicked dipole does not merely reduce to the earlier studied regime of the pattern formation by the individual solitons forming the dipole. With the further increase of k_0, the number of solitons in the output decreases by increasingly broad steps.

4.3.2 Dynamical Regimes Initiated by the Longitudinal Kick Applied to the Dipole

For the sake of the completeness of the description of the 2D system, we have also simulated essentially quasi-2D dynamical regimes initiated by the motion of the dipole kicked at angle of $\theta = \pi/2$, i.e., in the longitudinal direction, see (4.17). This setting implies the possibility to generate not only new dipoles but fundamental solitons as well. It was found that the minimum value of the kick which is necessary to set the dipole in motion is smaller in this case than the one given by (4.18):

$$k_0^{(\mathrm{thr})}\,(\theta = \pi/2) \approx 1.303. \tag{4.19}$$

The results obtained for this configuration are summarized in Table 4.1. Above the threshold value (4.19), additional moving solitons are created: one at $k_0 \in [1.304, 1.875]$ and two in a narrow interval $k_0 \in [1.880, 1.885]$. Then, for $k_0 \in [1.89, 2.015]$, a new moving dipole appears, which, as well as the original one, is oriented along the direction of the motion, and accompanied by two moving solitons. For $k_0 \in [2.02, 2.17]$, we have one moving soliton less, and at $k_0 \in [2.175, 2.255]$ the original dipole disappears in the course of the propagation, thus leaving one moving dipole and two moving solitons in the system. At $k_0 \in [2.26, 2.36]$, we observe the same pattern as for $k_0 \in [2.02, 2.17]$ (two dipoles and one moving soliton). Then, for $k_0 \in [2.365, 2.46]$, the dipole splits into two traveling solitons, with the upper one leaving a pinned soliton at the site which it originally occupied. At higher values of the kick's strength, the same pattern appears, except that the solitons do not leave anything behind them, just traveling through the lattice.

Table 4.1 The number of dipoles and fundamental solitons in the established pattern versus the kick's strength k_0 directed along the dipole's axis ($\theta = \pi/2$)

Behavior pattern	Range of k_0	Number of new solitons along the Y-direction
1 dipole	$k_0 \in [0, 1.303]$	0
1 dipole and 1 moving soliton	$k_0 \in [1.304, 1.875]$	1
1 dipole and 2 moving solitons	$k_0 \in [1.88, 1.885]$	2
2 dipoles and 2 moving solitons	$k_0 \in [1.89, 2.015]$	4
2 dipoles and 1 moving soliton	$k_0 \in [2.02, 2.17]$	3
1 dipole and 2 moving solitons	$k_0 \in [2.175, 2.255]$	2
2 dipoles and 1 moving soliton	$k_0 \in [2.26, 2.36]$	3
1pinned and 2 moving solitons	$k_0 \in [2.365, 2.46]$	1
2 moving solitons	$k_0 \in [2.465, \infty)$	0

In the right column, a newly emerging dipole (if any) is counted as two solitons

4.3.3 Collision Scenarios for Moving Dipoles in the System with Periodic Boundary Conditions

The above consideration was performed for a long system, before the collision of the freely moving dipole with the static pattern left in its wake, which should take place in the case of periodic b.c. In the application to laser-cavity settings, the periodic b.c. in the direction of X are relevant, corresponding to the cavity with the annular shape of its cross section. The study of dynamical pattern-formation scenarios with the periodic b.c. is also interesting in terms of the general analysis of models based on the complex GL equations [15].

Thus, under the periodic b.c., the freely moving dipole observed in Fig. 4.2 will complete the round trip and will hit the trapped chain of quiescent dipoles. Results of extensive simulations of this setting are summarized in the list of three different outcomes of the collisions, which feature persistent or transient dynamics (all the regimes were observed for $\theta = 0$, i.e., the transversely kicked dipole):

- The regime of periodic elastic collisions, corresponding to the periodically recurring passage of the moving dipole through the quiescent one, see Fig. 4.4. This outcome takes place for $k_0 \in [1.865, 1.868]$. Note that, according to Fig. 4.3, in this region the pattern left in the wake of the kicked dipole indeed amounts to another single quiescent dipole.
- The transient regime, which features several quasi-elastic collisions, before the moving dipole is eventually absorbed by the pinned pattern, which is a bound complex of two dipoles, see Fig. 4.5. This transient regime occurs around $k_0 = 1.816$, in which case Fig. 4.4 confirms that the moving dipole leaves a set of two additional dipoles in its wake.

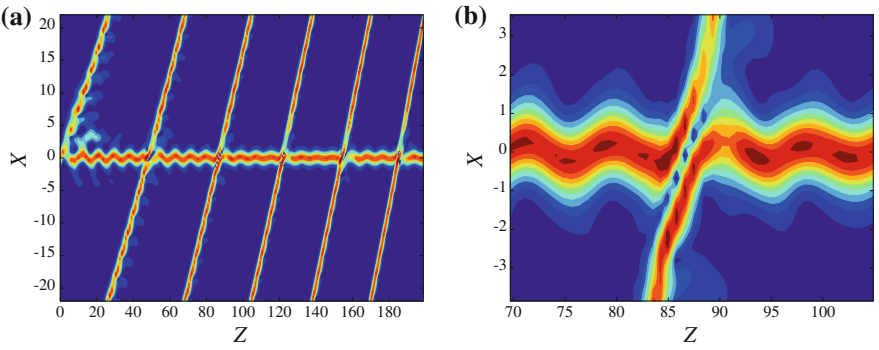

Fig. 4.4 **a** The cross section of field $|u\,(X, Y, Z)|$ at $Y = 0$, in the plane of (X, Z), for $k_0 = 1.865$. This is an example of the scenario of periodic elastic collisions, when the moving dipole repeats elastic collisions with the quiescent one. **b** The close-up of the elastic collision

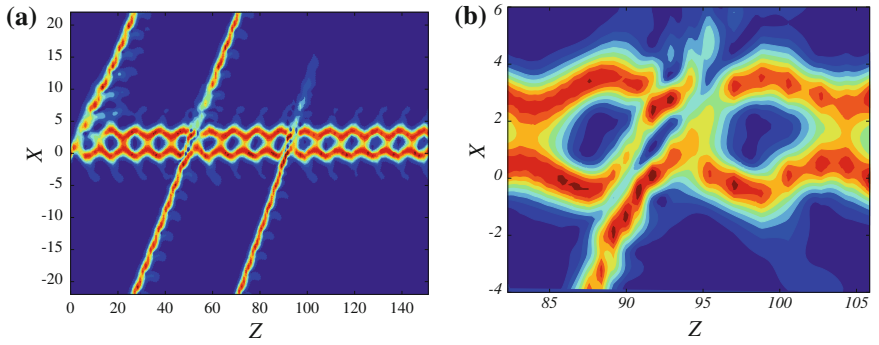

Fig. 4.5 **a** The cross section of field $|u\,(X, Y, Z)|$ at $Y = 0$, in the plane of (X, Z), for $k_0 = 1.816$. This is an example of the transient regime, when the moving dipole is absorbed by the pair of trapped ones after several quasi-elastic collisions. **b** The close-up of the absorptive collision

- The regime of "clearing the obstacle", opposite to the previous one: It features several elastic collisions, before the pinned dipole is absorbed by the moving one, see Fig. 4.6. This happens for $k_0 \in [1.884, 1.9]$ and around $k_0 = 2.083$ (in this region, Fig. 4.3 confirms that the moving dipole creates, originally, a single quiescent one).

In other cases, the freely moving dipole is absorbed by the quiescent pattern as a result of the first collision.

It is relevant to stress that, while the first two above-mentioned regimes have been reported in [15] for the motion of kicked fundamental solitons, the third regime ("clearing the obstacle") is a new one, which was not found for the fundamental solitons. Another characteristic feature of the latter regime is that it eventually leads to the splitting of the surviving single dipole into unbound fundamental solitons, as

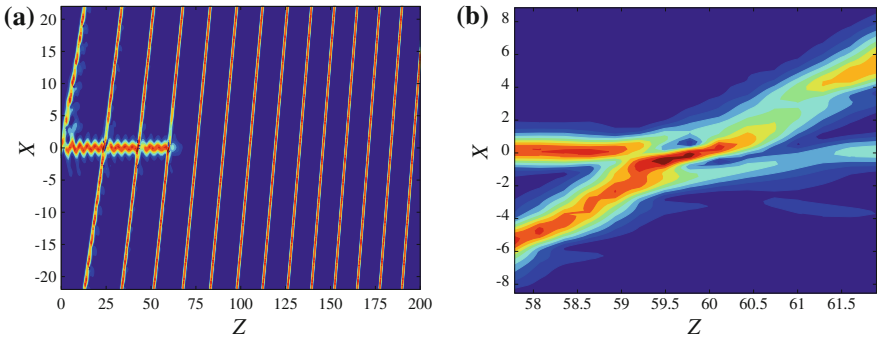

Fig. 4.6 **a** The cross section of field $|u(X, Y, Z)|$ at $Y = 0$, in the plane of (X, Z), for $k_0 = 1.884$. This is an example of "clearing the obstacle", when the moving dipole absorbs the stationary one, after several collisions with it. **b** The close-up of the absorptive collision

shown in Fig. 4.7a. To analyze the splitting, we have identified position $\{X_c, Y_c\}$ of the field maximum in each soliton (its center), and values of phases at these points (mod 2π), as functions of evolution variable Z. As a result, it has been found that the splitting of the dipole and the loss of the phase correlation between the splinters starts in a "latent form" at $Z \approx 102.8$, and becomes explicit at $Z \simeq 112.5$, see Fig. 4.7c, d. The two splinter solitons get completely separated at $Z \simeq 115$. The splitting also leads to the appearance of the velocity difference between the solitons (the velocity is defined as dX_c/dZ), as seen in Fig. 4.7b.

4.4 The Pattern Formation by Kicked Quadrupoles

A quadrupole is composed of four soliton-like power peaks, which are mutually locked with phase difference π between adjacent ones, see an example of the square-shaped (alias offsite-centered) quadrupole in Fig. 4.8. Although this mode carries no vorticity, simulations demonstrate that it is a very robust one. We here aim to investigate dynamical regimes initiated by the application of the horizontal kick (4.16) to the quadrupole.

The quadrupole is set in motion by the kick whose strength exceeds the respective threshold,

$$k_0^{(\mathrm{thr})}(\mathrm{quadr}) = 1.28, \tag{4.20}$$

cf. (4.18) and (4.19). The horizontal motion of the kicked quadrupole splits it into two vertical dipoles, and generates a set of additional vertically arranged quiescent *soliton pairs*, with a phase shift of $\pi/2$ between them. The dependence of the total number of solitons in the eventually established pattern on the kick's strength, k_0, is shown in Fig. 4.9. Because these simulations were subject to the periodic b.c., the free dipole completes the round trip to collide with the quiescent pattern. The

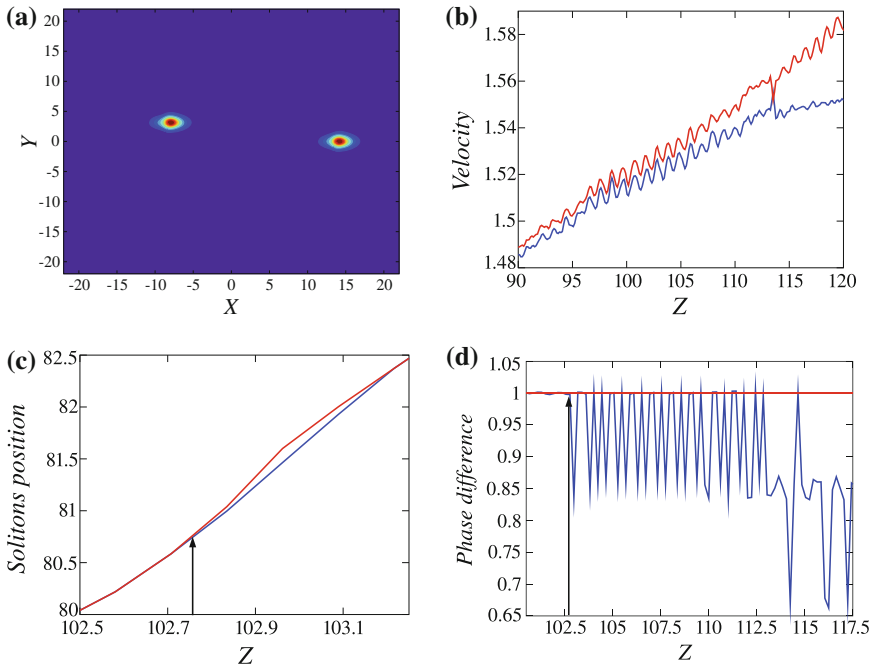

Fig. 4.7 Illustration of the splitting of the single surviving dipole into uncorrelated fundamental solitons, which follows "clearing the obstacle", after the absorption of the quiescent dipole by the moving one, at $k_0 = 1.884$. **a** Field $|u(X, Y)|$ at $Z = 199.965$. **b**, **c** Velocities and positions of both solitons as functions of Z. **d** The phase difference between the solitons versus Z, in units of π, the *red horizontal line* corresponding to the phase difference equal to π. The *arrows* in (**c**) and (**d**) indicate onset of the process which eventually leads to the loss of the phase coherence and separation of the two solitons

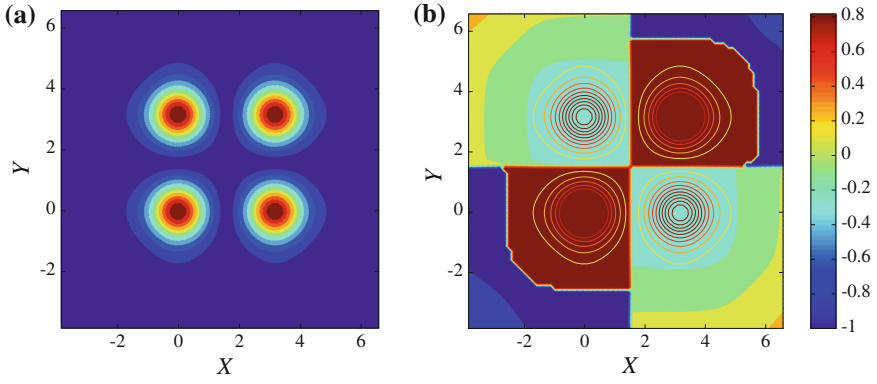

Fig. 4.8 The distribution of the amplitude (**a**) and phase (in unites of π) in the stable stationary square-shaped quadrupole used in the simulations (**b**)

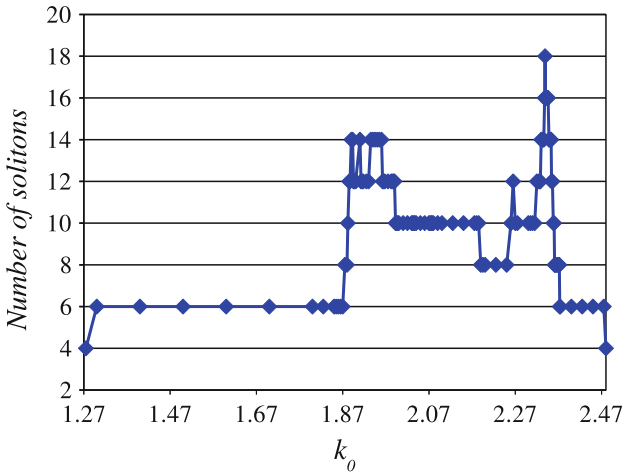

Fig. 4.9 The total number of fundamental solitons in the pattern produced by kick k_0 applied to the stable square-shaped quadrupole. Each dipole counts as two solitons

number of solitons was counted just before this collision. In the case where there is no motion in the system (no free dipole emerges), the count of the number of solitons is straightforward.

The result is quite different from that reported in the previous section for the pattern formation by the kicked dipole, cf. Fig. 4.3. Above the threshold value (4.20), the number of fundamental solitons in the emergent pattern increases and remains constant in a wide interval of values of k_0, *viz.*, six solitons for $k_0 \in [1.28, 1.87]$. Then, the number of the solitons increases to its maximum, which is 14 at $k_0 \in [1.89, 1.893]$, $k_0 = 1.91$ and $k_0 \in [1.935, 1.96]$. Note that the increase is not monotonous. For example, 12 solitons are generated at $k_0 = [1.885, 1.887]$ and $k_0 = [1.895, 1.9]$. Subsequently, in the interval of $k_0 \in [1.9125, 2.338]$, the soliton number varies between 8 and 16. The largest number of solitons, 18, is reached at $k_0 = 2.339$. Then, the soliton number drops to 6, and this value remains constant over a relatively broad interval, $k_0 \in [2.373, 2.475]$. At still larger values of k_0 , no additional solitons are generated by the initially moving quadrupole, which in this case again splits into two dipoles.

At $k_0 = 2.339$, the simulations generate a set of 18 solitons (the largest number, as said above). At first, two moving dipoles are actually produced by the splitting of the original quadrupole, see Fig. 4.10a. The faster dipole [whose trajectory is characterized by a larger slope (velocity), dX_c/dZ] moves without creating new solitons, while the slower one creates several of them, namely, the third moving dipole and six quiescent ones, which brings the total number of solitons to 18, as said above. The total energy increases up to about 24 times the energy of a quiescent soliton, which corresponds to the 12 such solitons, plus the 3 moving dipoles, with the energy of a moving soliton being about twice that of a quiescent one (see Fig. 4.10b). Due

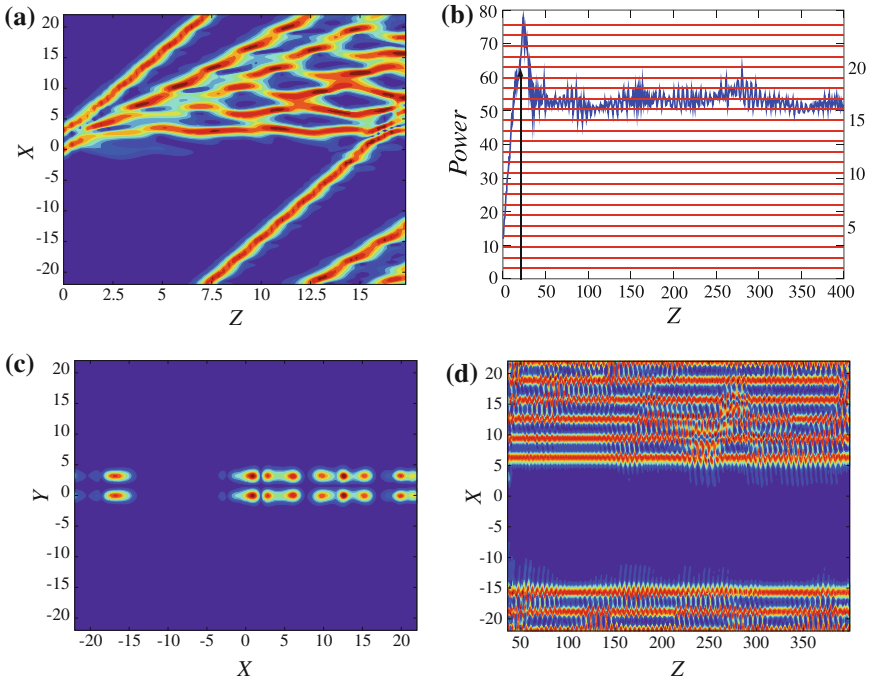

Fig. 4.10 The evolution of the horizontally kicked quadrupole, for $k_0 = 2.339$. **a** Field $|u\,(X, Y, Z)|$ in the cross section $Y = 0$, before the collision of the moving dipole with the pinned complex. **b** The total power versus Z (the *vertical arrow* indicates the collision point); the *horizontal red lines* show the power corresponding to n quiescent fundamental solitons, n being the numbers indicated on the *right vertical axis*. **c** Field $|u\,(X, Y)|$ at $Z = 399.34$. **d** Field $|u\,(X, Y, Z)|$ in the cross section $Y = 0$, after the collision

to the periodic b.c., the three moving dipoles hit the previously generated quiescent chain, one after the other (see Fig. 4.10a). As a result, two first dipoles are captured by the chain increasing the number of the bound solitons in it, while the third moving dipole is absorbed without adding new solitons to the chain. This complex interaction results in a chain of 8 quiescent dipoles (equivalent to 16 solitons). The so generated dipole train originally features intrinsic oscillations, which are eventually damped, see Fig. 4.10d. Note that Fig. 4.10a shows only the constituent fundamental solitons on line $Y = 0$, in terms of Fig. 4.10c, their counterparts on the line of $Y = 3$ showing the same picture.

As mentioned above and shown in Fig. 4.11, at $k_0 > 2.48$ the initial quadrupole splits into two dipoles, which move at different velocities, without the formation of additional soliton pairs. Each dipole keeps the phase difference of π between the constituent solitons (the jumps are due to a numerical uncertainty).

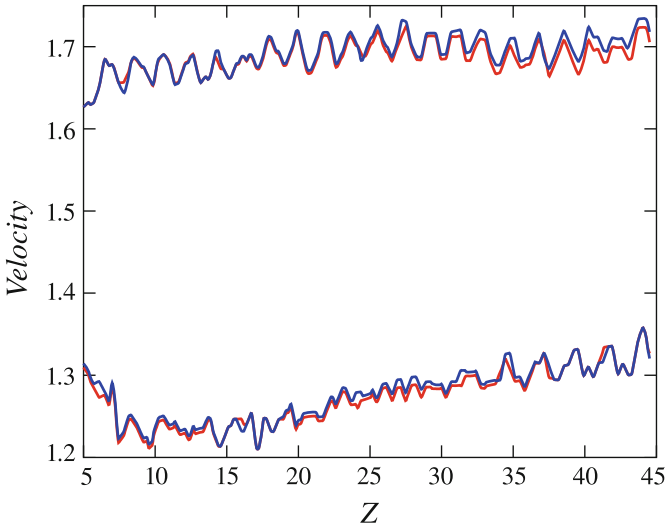

Fig. 4.11 Velocities of two dipoles into which the kicked quadrupole splits at $k_0 = 3$

4.5 The Pattern Formation by Kicked Vortices

It is well known that the lattice potential supports localized vortical modes of two types, rhombuses and squares, alias the onsite- and offsite-centered ones [12, 68, 101, 102]. Continuing the analysis presented in the previous sections, here we address the mobility of vortices, and formation of structures in the wake of moving ones.

4.5.1 Chaotic Patterns Generated by Kicked Rhombic (Onsite-Centered) Vortices

First, we consider the pattern-formation dynamics for horizontally kicked rhombic vortices built of four fundamental solitons with an empty site in the center, which carry the total phase circulation of 2π, corresponding to the topological charge $S = 1$, see Fig. 4.12a.

A weak horizontal kick, with $k_0 \lesssim 0.1$, excites oscillations of the constituent fundamental solitons which built the vortex, while vorticity $S = 1$ is kept (i.e., phase differences between the adjacent solitons remain very close to $\pi/2$), see Fig. 4.13b. A stronger kick (for instance, $k_0 = 0.5$) destroys the vortical phase structure, and transforms the vortex into a quadrupole, as shown in Fig. 4.13c.

At $k_0 = 1.0$ and $k_0 = 1.5$, see Fig. 4.14a, b, respectively, the kick completely destroys the vortices, which are replaced by apparently random clusters of quiescent fundamental solitons. Note that, although the results shown in Fig. 4.14a,b have been

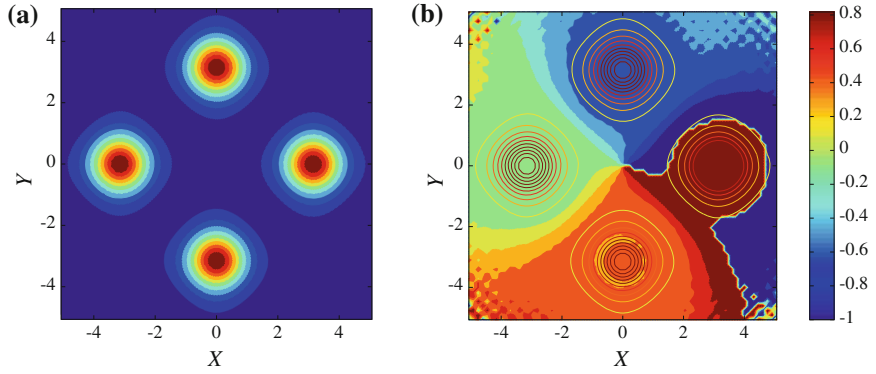

Fig. 4.12 **a** and **b** The distribution of the amplitude and phase (in units of π) in the stable rhombus-shaped (onsite-centered) vortex

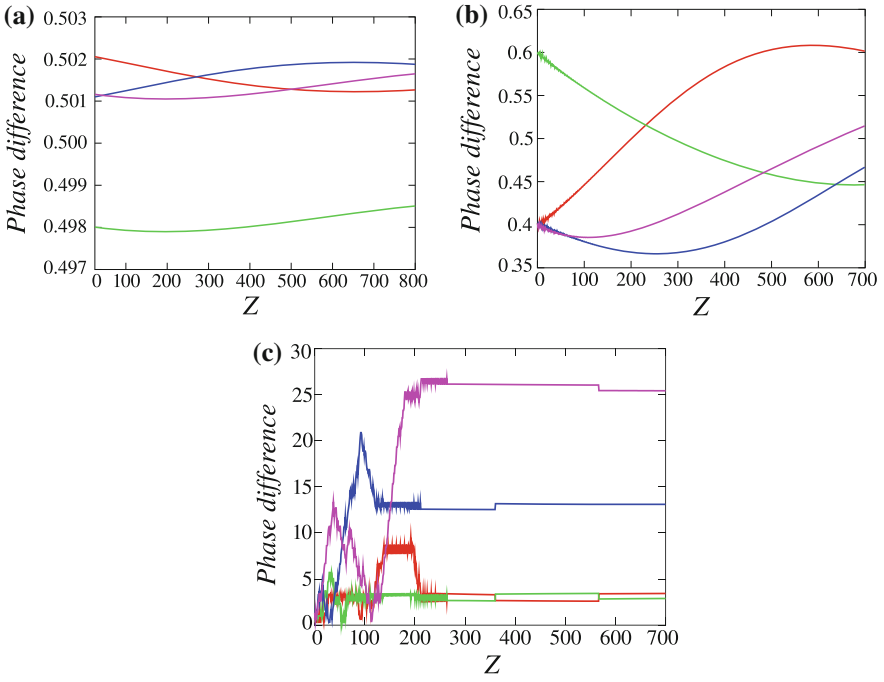

Fig. 4.13 The phase difference between adjacent constituent solitons (in units of π), versus Z, in a weakly kicked rhombic vortex, for different values of the kick's strength: **a** $k_0 = 0$, **b** $k_0 = 0.1$, **c** $k_0 = 0.2$

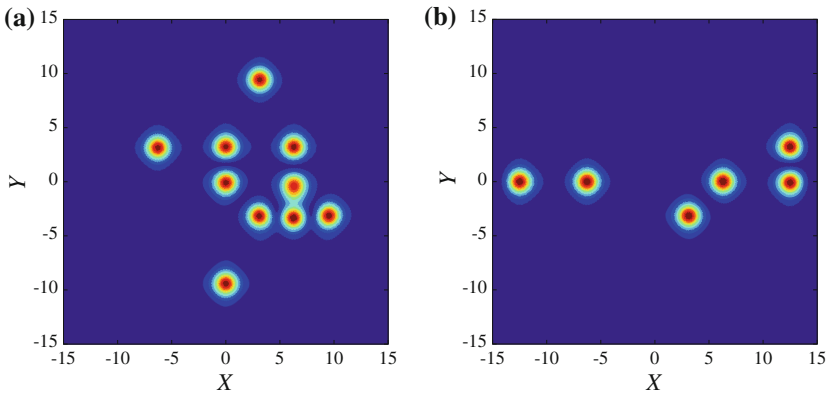

Fig. 4.14 **a** Field $|u\,(X, Y)|$ at $Z = 299.725$, generated by the kicked rhombic vortex for $k_0 = 1.0$. **b** The same as in Fig. 4.14a , but for $k_0 = 1.5$

obtained with absorbing b.c., rather than periodic ones, this circumstance does not affect the results. The same type of b.c. is used below.

4.5.2 Kicked Square-Shaped (Offsite-Centered) Vortices

Unlike their rhombic counterparts, quiescent square-shaped vortices, such as the one shown in Fig. 4.15, are unstable in the entire parameter space of (4.14) which we have explored, in agreement with the general trend of the offsite-centered vortices to be more fragile than their onsite-centered counterparts [68]. As a result of the instability development, they are transformed into stable quadrupoles. Nevertheless, results displayed below confirm that it is relevant to consider dynamical pattern formation by unstable kicked vortices as this type.

First, we consider the application of the horizontal kick (4.16) corresponding to $\theta = 0$ and varying strength k_0. The fundamental solitons building the vortex oscillate without setting in progressive motion below the threshold, $k_0 \leq k_0^{(\mathrm{thr})} = 1.2125$, cf. (4.18), (4.19), and (4.20). Actually, it may happen, in this case, that a new soliton is created and starts moving in the horizontal direction, but the energy is not sufficient to stabilize it, and the new soliton decays eventually, while the initial solitons which compose the square-shaped vortex are recovered at the original positions. The inner phase structure of the unstable square-shaped vortices is destroyed in the course of the oscillations, and it transforms into a quadrupole, in accordance with the above-mentioned fact that this is the outcome of its instability in the absence of the kick.

The increase of k_0 leads to formation of new 2D patterns. At $k_0 = 1.5$, the right vertical pair (column) of the fundamental solitons, which are a part of the original vortical square, start to duplicate themselves, while moving to the right (in the direction of the kick), see Fig. 4.16. A noteworthy effect is breaking of the

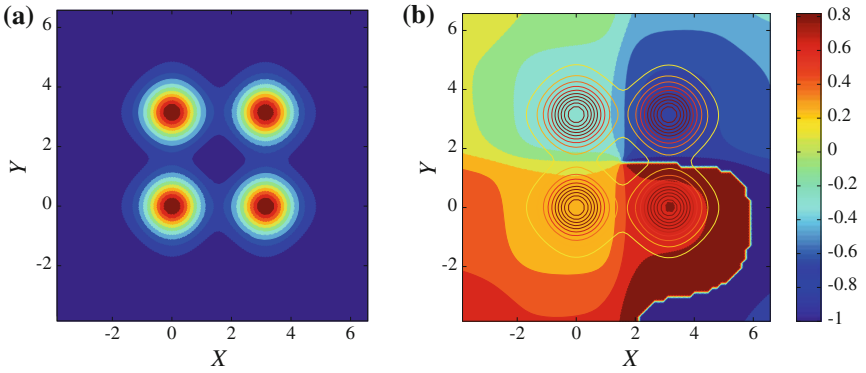

Fig. 4.15 The distribution of the amplitude (**a**) and phase (**b**) in the unstable square-shaped (offsite-centered) vortex

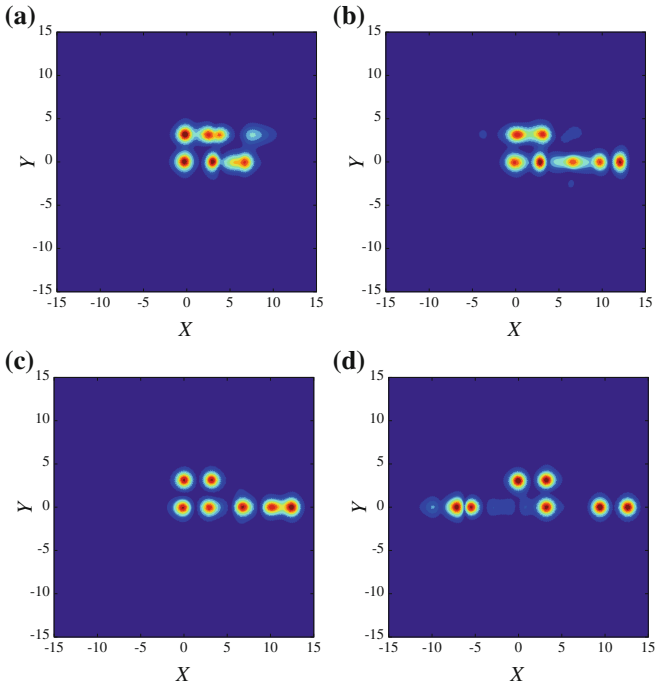

Fig. 4.16 The evolution of the unstable square-shaped (offsite-centered) vortex kicked in the horizontal direction ($\theta = 0$) with $k_0 = 1.5$. **a** $Z = 2.6593$, **b** $Z = 12.008$, **c** $Z = 239.91$, **d** $Z = 299.825$

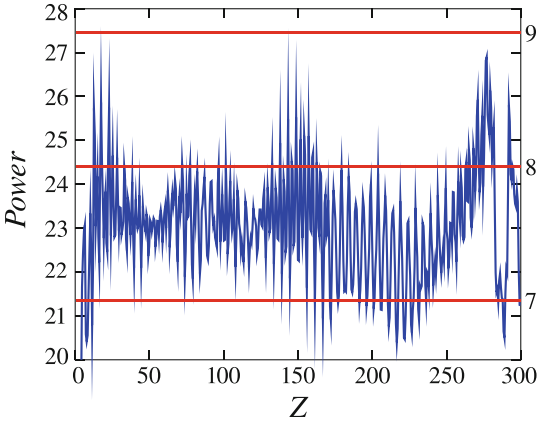

Fig. 4.17 The evolution of the total power for the pattern produced by horizontally kicking the square-shaped vortex, for $k_0 = 1.5$. The *red horizontal lines* show power levels corresponding to n quiescent solitons

symmetry between the top and bottom solitons in the column by the kick, only the bottom soliton succeeding to create a horizontal array of additional solitons (three ones, in total). In this case, Fig. 4.17 shows that the eventual value of the total power (4.15) oscillates between values corresponding to the cumulative power of 7 or 8 quiescent fundamental solitons. The resulting pattern develops a disordered form, which keeps to oscillate randomly, as Fig. 4.17 clearly demonstrate.

At somewhat higher values of k_0 (for example, $k_0 = 2.0$), the original four-soliton set is transformed into a quiescent three-soliton complex, while an extra dipole and separate free solitons are created and travel through the lattice, see Fig. 4.18.

Finally, a still stronger kick applied to the square vortex transforms it into a square-shaped cluster of four solitons moving as a whole, see Fig. 4.19a, b, which display the result in the 3D form. In the former case, at $k_0 = 2.5$, the cluster leaves behind a copy of one of the original solitons, while at $k_0 = 3.0$ the moving cluster is the single emerging mode. Although the clusters are dynamically stable, they do not carry the vortical phase structure.

We have also studied the application of the kick to the square-shaped vortex in other directions, i.e., varying angle θ in (4.17). First, as seen in Fig. 4.20a, in the case of $\theta = \pi/8$ and $k_0 = 1.5$, the kick again breaks the symmetry between the top and bottom rows of the solitons, generating an array of additional solitons in the bottom horizontal row. Further, to check that the numerical code is compatible with the global symmetry of the setting, we also considered equivalent angles, $\theta = 5\pi/8, 9\pi/8$ and $13\pi/8$. The results, shown in Fig. 4.20, evidence the possibility of controlling the direction of the emission of the soliton array by the direction of the initial kick.

Further, running the computations for varying θ and moderate values of k_0, we have concluded that there is a threshold angle ε , so that the emission towards any of the four equivalent directions, corresponding to directions $\phi = 0, \pi/2, \pi$ or $3\pi/2$, occurs provided that the orientation of the kick belongs to a certain range around this direction, *viz.*, $(\phi - \pi/4 + \varepsilon) < \theta < (\phi + \pi/4 - \varepsilon)$, with $\varepsilon = 0.059$. If the

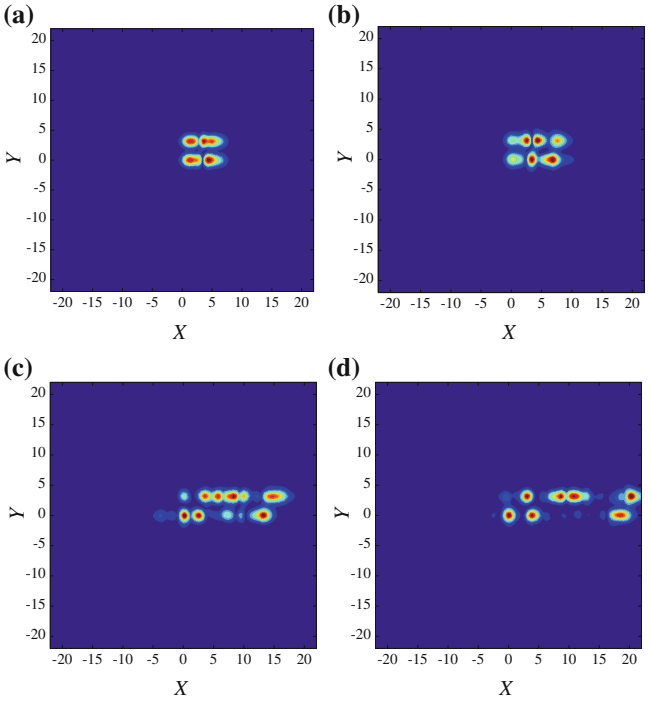

Fig. 4.18 The evolution pattern produced by horizontally kicking the square-shaped vortex, for $k_0 = 2$. **a** $Z = 1.0784$, **b** $Z = 20.680$, **c** $Z = 5.1432$, **d** $Z = 7.5069$

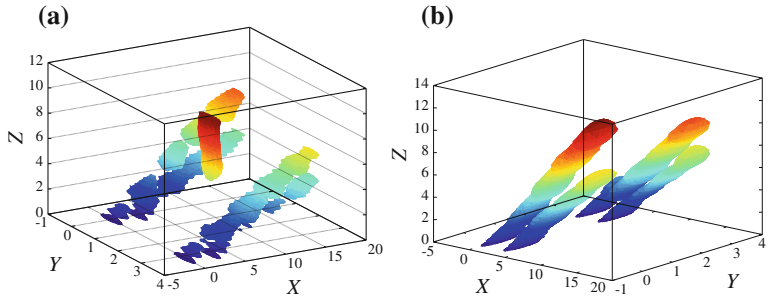

Fig. 4.19 **a** The three-dimensional rendition of the evolution of the horizontally kicked square-shaped vortex for $k_0 = 2.5$, which is transformed into a stably moving four-soliton cluster. The *chromatic progression* indicates the propagation direction. The *vertical rod* represents the additional quiescent fundamental soliton, *left* in the wake of the moving four-soliton cluster. **b** The same as in Fig. 4.19a but for $k_0 = 3.0$. In this case, the unstable vortex is entirely transformed into the stable moving cluster

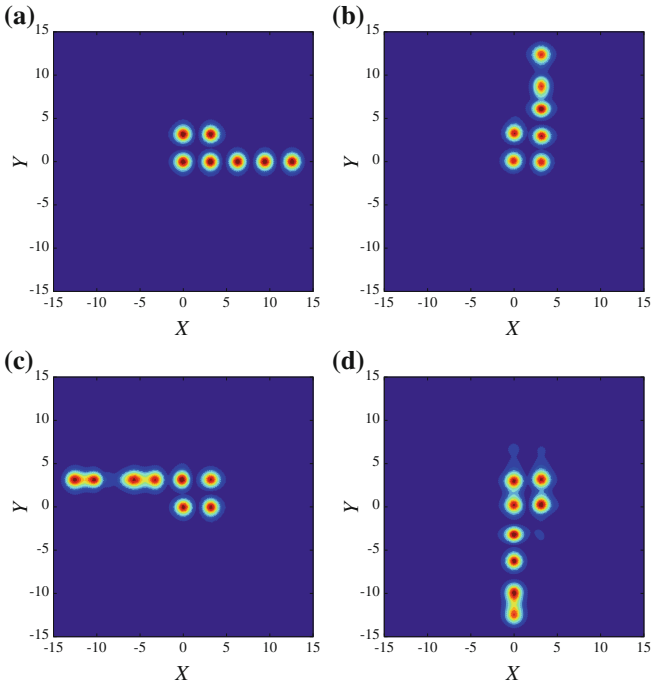

Fig. 4.20 The pattern produced by the square-shaped vortex kicked with strength $k_0 = 1.5$ in different but actually equivalent directions: **a** $\theta = \pi/8$; **b** $\theta = 5\pi/8$; **c** $\theta = 9\pi/8$; **d** $\theta = 13\pi/8$

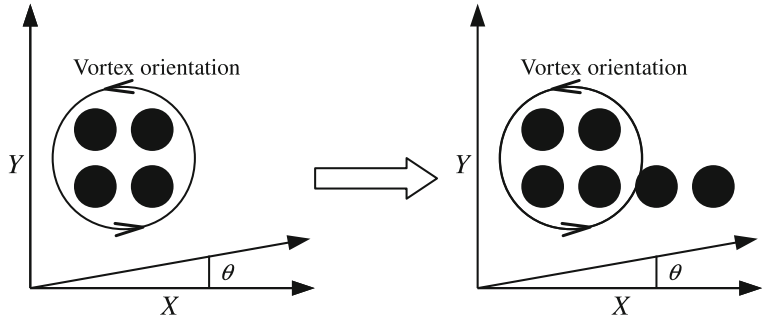

Fig. 4.21 The explanation of the direction in which the soliton array is emitted from the kicked square-shaped vortex

kick's orientation falls into interstices between these ranges, namely,$[\phi + \pi/4 - \varepsilon; \phi + \pi/4 + \varepsilon]$, solitons arrays are not generated. In the latter case, the square vortex transforms into a quadrupole.

These results can be explained by noting that the intrinsic phase circulation in the vortex is directed counterclockwise (from X to Y). Then, as schematically shown (for example) for $\theta = \pi/8$ in Fig. 4.21, the superposition of the externally applied

kick (the phase gradient) and the intrinsic phase flow gives rise to the largest local phase gradient at the position of the bottom right soliton, in the positive horizontal direction, therefore the array is emitted accordingly.

4.6 Conclusions

The objective of this chapter is to extend the analysis of the dynamical pattern-formation scenarios in the cubic-quintic complex GL (Ginzburg-Landau) equation with the cubic-quintic nonlinearity and 2D cellular potential. This problem is related to the general theme of the present volume, *viz.*, mobility of localized modes in lattice potentials.

The cubic-quintic complex GL equation is the model for laser cavities with built-in gratings, represented by the spatially periodic potential. Recently, the quasi-1D pattern-formation scenarios, initiated by the moving fundamental solitons, were studied in this model. Here, we have systematically analyzed the fully 2D scenarios, produced by kicking compound modes, *viz.*, dipoles, offsite-centered quadrupoles, and vortices of two different types (onsite- and offsite-centered rhombuses and squares). The motion of the kicked compound through the cellular potential leads to the generation of diverse multi-peak patterns pinned to the lattice, which the moving object leaves in its wake. In the annular system with periodic boundary conditions, the persistently traveling dipole hits the pinned pattern from the opposite direction. In this way, several dynamical regimes are initiated, including the periodically recurring elastic passage of the free dipole through the quiescent one, and transient regimes, which lead, after a few quasi-elastic collisions, to absorption of one dipole by the other. In the case of vortices, the dependence of the outcome on the magnitude and direction of the kick was investigated too. In particular, a noteworthy result is that a strong kick transforms the original squared-shaped vortex (which is unstable by itself) into a clean stably moving four-soliton cluster.

Acknowledgments The work of DM was supported in part by a Senior Chair Grant from the Ré gion Pays de Loire, France.

References

1. Abdullaev, F.K., Konotop, V.V., Salerno, M., Yulin, A.V.: Dissipative periodic waves, solitons, and breathers of the nonlinear Schrödinger equation with complex potentials. Phys. Rev. E **82**, 056606 (2010)
2. Afanasjev, V.V., Akhmediev, N., Soto-Crespo, J.M.: Three forms of localized solutions of the quintic complex Ginzburg-Landau equation. Phys. Rev. E **53**(2), 1931–1939 (1996)
3. Akhmediev, N., Afanasjev, V.V.: Novel arbitrary-amplitude soliton solutions of the cubic-quintic complex Ginzburg-Landau equation. Phys. Rev. Lett. **75**(12), 2320–2323 (1995)
4. Akhmediev, N., Ankiewicz (eds.): Dissipative Solitons: From Optics to Biology, Medicine. Lecture Notes in Physics, vol. 751. Springer, New York (2008)

5. Akhmediev, N., Ankiewicz, A. (eds.): Dissipative Solitons. Springer, New York (2005)
6. Aleksić, N.B., Skarka, V., Timotijević, D.V., Gauthier, D.: Self-stabilized spatiotemporal dynamics of dissipative light bullets generated from inputs without spherical symmetry in three-dimensional Ginzburg-Landau systems. Phys. Rev. A **75**, 061802(R) (2007)
7. Anglin, J.: Cold, dilute, trapped bosons as an open quantum system. Phys. Rev. Lett. **79**(1), 6–9 (1997)
8. Aranson, I.S., Kramer, L.: The world of the complex Ginzburg-Landau equation. Rev. Mod. Phys. **74**, 99–143 (2002)
9. Arecchi, F.T., Bragard, J., Castellano, L.M.: Dissipative dynamics of an open Bose-Einstein condensate. Opt. Commun. **179**(1–6), 149–156 (2000)
10. Atai, J., Malomed, B.A.: Stability and interactions of solitons in two-component active systems. Phys. Rev. E **54**, 4371–4374 (1996)
11. Atai, J., Malomed, B.A.: Exact stable pulses in asymmetric linearly coupled Ginzburg-Landau equations. Phys. Lett. A **246**(5), 412–422 (1998)
12. Baizakov, B.B., Malomed, B.A., Salerno, M.: Multidimensional solitons in periodic potentials. Europhys. Lett. **63**(5), 642–648 (2003)
13. Bakonyi, Z., Michaelis, D., Peschel, U., Onishchukov, G., Lederer, F.: Dissipative solitons and their critical slowing down near a supercritical bifurcation. J. Opt. Soc. Am. B **19**(3), 487–491 (2002)
14. Barland, S., Tredicce, J.R., Brambilla, M., Lugiato, L.A., Balle, S., Giudici, M., Maggipinto, T., Spinelli, L., Tissoni, G., Knödl, T., Miller, M., Jäger, R.: Cavity solitons as pixels in semiconductor microcavities. Nature **419**, 699–701 (2002)
15. Besse, V., Leblond, H., Mihalache, D., Malomed, B.A.: Pattern formation by kicked solitons in the two-dimensional Ginzburg-Landau medium with a transverse grating. Phys. Rev. E **87**, 012916 (2013)
16. Besse, V., Leblond, H., Mihalache, D., Malomed, B.A.: Building patterns by traveling dipoles and vortices in two-dimensional periodic dissipative media. Opt. Commun. **332**, 279–291 (2014)
17. Bliokh, K.Y., Bliokh Y. P. a. andnd Ferrando, A.: Resonant plasmon-soliton interaction. Phys. Rev. A **79**, 041803(R) (2009)
18. Borovkova, O., Kartashov, Y.V., Vysloukh, V.A., Lobanov, V.E., Malomed, B.A., Torner, L.: Solitons supported by spatially and inhomogeneous nonlinear losses. Opt. Exp. **20**(3), 2657–2667 (2012)
19. Borovkova, O.V., Kartashov, Y.V., Lobanov, V.E., Vysloukh, V.A., Torner, L.: Vortex twins and anti-twins supported by multiring gain landscapes. Opt. Lett. **36**(19), 3783–3785 (2011)
20. Borovkova, O.V., Lobanov, V.E., Kartashov, Y.V., Torner, L.: Rotating vortex solitons supported by localized gain. Opt. Lett. **36**, 1936–1938 (2011)
21. Borovkova, O.V., Lobanov, V.E., Kartashov, Y.V., Torner, L.: Stable vortex-soliton tori with multiple nested phase singularities in dissipative media. Phys. Rev. A **85**, 023814 (2012)
22. Borovkova, O.V., Lobanov, V.E., Malomed, B.A.: Stable nonlinear amplification of solitons without gain saturation. Europhys. Lett. **97**(4), 44003 (2012)
23. Brand, H.R., Deissler, R.J.: Interaction of localized solutions for subcritical bifurcations. Phys. Rev. Lett. **63**(26), 2801–2804 (1989)
24. Crasovan, L.C., Malomed, B.A., Mihalache, D.: Erupting, flat-top, and composite spiral solitons in the two-dimensional Ginzburg-Landau equation. Phys. Lett. A **289**(1–2), 59–65 (2001)
25. Crasovan, L.C., Malomed, B.A., Mihalache, D.: Stable vortex solitons in the two-dimensional Ginzburg-Landau equation. Phys. Rev. E **63**, 016605 (2001)
26. Cross, M.C., Hohenberg, P.C.: Pattern formation outside of equilibrium. Rev. Mod. Phys. **65**, 851–112 (1993)
27. Das, S.K., Puri, S., Cross, M.C.: Nonequilibrium dynamics of the complex Ginzburg-Landau equation: analytical results. Phys. Rev. E **64**, 046206 (2001)
28. Davoyan, A.R., Shadrivov, I.V., Kivshar, Y.S.: Self-focusing and spatial plasmon-polariton solitons. Opt. Exp. **17**, 21732–21737 (2009)

29. Fauve, S., Thual, O.: Solitary waves generated by subcritical instabilities in dissipative systems. Phys. Rev. Lett. **64**(3), 282–284 (1990)
30. Fedorov, S.V., Vladimirov, A.G., Khodova, G.V., Rosanov, N.N.: Effect of frequency detunings and finite relaxation rates on laser localized structures. Phys. Rev. E **61**(5), 5814–5824 (2000)
31. Feigenbaum, E., Orenstein, M.: Plasmon-soliton. Opt. Lett. **32**(6), 674–676 (2007)
32. Fernandez-Oto, C., Clerc, M.G., Escaff, D., Tlidi, M.: Strong nonlocal coupling stabilizes localized structures: an analysis based on front dynamics. Phys. Rev. Lett. **110**, 174101 (2013)
33. Firth, W.J., Scroggie, A.J.: Optical bullet holes: robust controllable localized states of a nonlinear cavity. Phys. Rev. Lett. **76**(10), 1623–1626 (1996)
34. Fleischer, J.W., Segev, M., Efremidis, N.K., Christodoulides, D.N.: Observation of two-dimensional discrete solitons in optically induced nonlinear photonic lattices. Nature **422**, 147–150 (2003)
35. Gabitov, I.R., Korotkevich, A.O., Maimistov, A.I., McMahon, J.B.: Solitary waves in plasmonic Bragg gratings. Appl. Phys. A **89**, 277–281 (2007)
36. Genevet, P., Barland, S., Giudici, M., Tredicce, J.R.: Bistable and addressable localized vortices in semiconductor lasers. Phys. Rev. Lett. **104**, 223902 (2010)
37. Grelu, P., Akhmediev, N.: Dissipative solitons for mode-locked lasers. Nat. Photonics **6**(2), 84–92 (2012)
38. Hakim V., Jakobsen, P., Pomeau, Y.: Fronts versus solitary waves in nonequilibrium systems. Europhys. Lett. **11**, 19 (1990)
39. Hoffmann, K.H., Tang, Q.: Ginzburg-Landau Phase Transition Theory and Superconductivity. Birkhauser, Basel (2001)
40. Huang, C., Ye, F., Malomed, B.A., Kartashov, Y.V., Chen, X.: Solitary vortices supported by localized parametric gain. Opt. Lett. **38**(13), 2177–2180 (2013)
41. Hukriede, J., Runde, D., Kip, D.: Fabrication and application of holographic Bragg gratings in lithium niobate channel waveguides. J. Phys. D **36**(3), R1–R16 (2003)
42. He, Y.J., Malomed, B.A., Mihalache, D., Ye, F.W., Hu, B.B.: Generation of arrays of spatiotemporal dissipative solitons by the phase modulation of a broad beam. J. Opt. Soc. Am. B **27**(6), 1266–1271 (2010)
43. Jiménez, J., Noblet, Y., Paulau, P.V., Gomila, D., Ackemann, T.: Observation of laser vortex solitons in a self-focusing semiconductor laser. J. Opt. **15**(4), 044011 (2013)
44. Kartashov, Y.V., Konotop, V.V., Vysloukh, V.A., Zezyulin, D.A.: Guided modes and symmetry breaking supported by localized gain. In: Malomed, B.A. (ed.) Spontaneous Symmetry Breaking, Self-Trapping, and Josephson Oscillations. Springer, New York (2013)
45. Kartashov, Y.V., Konotop, V.V., Vysloukh, V.V.: Dissipative surface solitons in periodic structures. Europhys. Lett. **91**, 340003 (2010)
46. Kazantseva, E.V., Maimistov, A.I.: Polaritonic gap-soliton propagation through a wide defect in a resonantly absorbing Bragg grating. Phys. Rev. A **79**, 033812 (2009)
47. Keeling, J., Berloff, N.G.: Spontaneous rotating vortex lattices in a pumped decaying condensate. Phys. Rev. Lett. **100**, 250401 (2008)
48. Kolodner, P., Glazier, J.A., Williams, H.: Dispersive chaos in one-dimensional traveling-wave convection. Phys. Rev. Lett. **65**(13), 1579–1582 (1990)
49. Lazarides, N., Tsironis, G.P.: Coupled nonlinear Schrödinger field equations for electromagnetic wave propagation in nonlinear left-handed materials. Phys. Rev. E **71**, 036614 (2005)
50. Leblond, H., Komarov, A., Salhi, M., Haboucha, A., Sanchez, F.: <cis>bound states of three localized pulses of the cubic-quintic complex Ginzburg-Landau equation. J. Opt. A: Pure Appl. Opt. **8**(3), 319 (2006)
51. Leblond, H., Malomed, B.A., Mihalache, D.: Stable vortex solitons in the Ginzburg-Landau model of a two-dimensional lasing medium with a transverse grating. Phys. Rev. A **80**, 033835 (2009)
52. Lin, Y.Y., Lee, R.K., Kivshar, Y.: Transverse instability of transverse-magnetic solitons and nonlinear surface plasmons. Opt. Lett. **34**(19), 2982–2984 (2009)

53. Liu, Y.M., Bartal, G., Genov, D.A., Zhang, X.: Subwavelength discrete solitons in nonlinear metamaterials. Phys. Rev. Lett. **99**, 153901 (2007)
54. Lobanov, V.E., Kartashov, Y.V., Vysloukh, V.A., Torner, L.: Stable radially symmetric and azimuthally modulated vortex solitons supported by localized gain. Opt. Lett. **36**, 85–87 (2011)
55. Lugiato, L.A., Brambilla, M., Gatti, A.: Optical pattern formation. Adv. At. Molec. Opt. Phys. **40**, 229–306 (1999)
56. Mak, W.C.K., Malomed, B.A., Chu, P.L.: Interaction of a soliton with a localized gain in a fiber Bragg grating. Phys. Rev. E **67**, 026608 (2003)
57. Malomed, B.A.: Evolution of nonsoliton and "quasi-classical" wavetrains in nonlinear Schrödinger and Korteweg - de Vries equations with dissipative perturbations. Physica D **29**(1–2), 155–172 (1987)
58. Malomed, B.A.: Complex Ginzburg-Landau equation. In: Scott, A. (ed.) Encyclopedia of Nonlinear Science. Routledge, New York (2005)
59. Malomed, B.A.: Solitary pulses in linearly coupled Ginzburg-Landau equations. Chaos **17**(3), 037117 (2007)
60. Malomed, B.A.: Spatial solitons supported by localized gain. J. Opt. Soc. Am. B **31**, 2460–2475 (2014)
61. Malomed, B.A., Dzyapko, O., Demidov, V.E., Demokritov, S.O.: Ginzburg-Landau model of Bose-Einstein condensation of magnons. Phys. Rev. B **81**, 024418 (2010)
62. Malomed, B.A., Nepomnyashchy, A.A.: Kinks and solitons in the generalized Ginzburg-Landau equation. Phys. Rev. A **42**, 6009 (1990)
63. Malomed, B.A., Winful, H.G.: Stable solitons in two-component active systems. Phys. Rev. E **53**, 5365–5368 (1996)
64. Mandel, P., Tlidi, M.: Transverse dynamics in cavity nonlinear optics (2000–2003). J. Opt. B: Quantum Semiclass. Opt. **6**, R60 (2004)
65. Marcq, P., Chaté, H., Conte, R.: Exact solutions of the one-dimensional quintic complex Ginzburg-Landau equation. Physica D **73**(4), 305–317 (1994)
66. Marini, A., Skryabin, D.V.: Ginzburg-Landau equation bound to the metal-dielectric interface and transverse nonlinear optics with amplified plasmon polaritons. Phys. Rev. A **81**, 033850 (2010)
67. Marini, A., Skryabin, D.V., Malomed, B.A.: Stable spatial plasmon solitons in a dielectric-metal-dielectric geometry with gain and loss. Opt. Exp. **19**(7), 6616–6622 (2011)
68. Mayteevarunyoo, T., Malomed, B.A., Baizakov, B.B., Salerno, M.: Matter-wave vortices and solitons in anisotropic optical lattices. Physica D **238**(15), 1439–1448 (2009)
69. Mejia-Cortes, C., Soto-Crespo, J.M., Vicencio, R.A., Molina, M.I.: Vortex solitons of the discrete Ginzburg-Landau equation. Phys. Rev. A **83**, 043837 (2011)
70. Mihalache, D.: Three-dimensional Ginzburg-Landau dissipative solitons supported by a two-dimensional transverse grating. Proc. Rom. Acad. A **11**, 142–147 (2010)
71. Mihalache, D.: Spiral solitons in two-dimensional complex cubic-quintic Ginzburg-Landau models. Rom. Rep. Phys. **63**, 325–338 (2011)
72. Mihalache, D.: Linear and nonlinear light bullets: recent theoretical and experimental studies. Rom. J. Phys. **57**(1–2), 352–371 (2012)
73. Mihalache, D., Mazilu, D.: Ginzburg-Landau spatiotemporal dissipative optical solitons. Rom. Rep. Phys. **60**(3), 749–762 (2008)
74. Mihalache, D., Mazilu, D., Lederer, F., Kartashov, Y.V., Crasovan, L.C., Torner, L., Malomed, B.A.: Stable vortex tori in the three-dimensional cubic-quintic Ginzburg-Landau equation. Phys. Rev. Lett. **97**, 073904 (2006)
75. Mihalache, D., Mazilu, D., Lederer, F., Leblond, H., Malomed, B.A.: Stability limits for three-dimensional vortex solitons in the Ginzburg-Landau equation with the cubic-quintic nonlinearity. Phys. Rev. A **76**, 045803 (2007)
76. Mihalache, D., Mazilu, D., Lederer, F., Leblond, H., Malomed, B.A.: Stability of dissipative optical solitons in the three-dimensional cubic-quintic Ginzburg-Landau equation. Phys. Rev. A **75**, 033811 (2007)

77. Mihalache, D., Mazilu, D., Lederer, F., Leblond, H., Malomed, B.A.: Spatiotemporal solitons in the Ginzburg-Landau model with a two-dimensional transverse grating. Phys. Rev. A **81**, 025801 (2010)
78. Mihalache, D.a., Mazilu, D., Skarka, V., Malomed, B.A., Leblond, H., Aleksić, N.B., Lederer, F.: Stable topological modes in two-dimensional Ginzburg-Landau models with trapping potentials. Phys. Rev. A **82**, 023813 (2010)
79. Pereira, N.R., Stenflo, L.: Nonlinear Schrödinger equation including growth and damping. Phys. Fluids **20**, 1733–1734 (1977)
80. Petviashvili, V.I., Sergeev, A.M.: Spiral solitons in active media with an excitation threshold. Dokl. AN SSSR- Sov. Phys. Doklady **276**,(29), 493, 1380–1384 (1984)
81. Renninger, W.H., Chong, A., Wise, F.W.: Dissipative solitons in normal-dispersion fiber lasers. Phys. Rev. A **77**, 023814 (2008)
82. Rosanov, N.N.: Spatial Hysteresis and Optical Patterns. Springer, New York (2002)
83. Rosanov, N.N., Fedorov, S.V., Shatsev, A.N.: Two-dimensional laser soliton complexes with weak, strong, and mixed coupling. Appl. Phys. B **81**(7), 937–943 (2005)
84. Sakaguchi, H.: Motion of pulses and vortices in the cubic-quintic complex Ginzburg-Landau equation without viscosity. Physica D **210**(1–2), 138–148 (2005)
85. Schöpf, W., Kramer, L.: Small-amplitude periodic and chaotic solutions of the complex Ginzburg-Landau equation for a subcritical bifurcation. Phys. Rev. Lett. **66**, 2316–2319 (2003)
86. Skarka, V., Aleksić, N., Leblond, H., Malomed, B.A., Mihalache, D.: Varieties of stable vortical solitons in Ginzburg-Landau media with radially inhomogeneous losses. Phys. Rev. Lett. **105**, 213901 (2010)
87. Skarka, V., Aleksić, N.B.: Stability criterion for dissipative soliton solutions of the one-, two-, and three-dimensional complex cubic-quintic Ginzburg-Landau equations. Phys. Rev. Lett. **96**, 013903 (2006)
88. Skarka, V., Timotijević, D.V., Aleksić, N.B.: Extension of the stability criterion for dissipative optical soliton solutions of a two-dimensional Ginzburg-Landau system generated from asymmetric inputs. J. Opt. A: Pure Appl. Opt. **10**, 075102 (2008)
89. Soto-Crespo, J.M., Akhmediev, N., Ankiewicz, A.: Pulsating, creeping, and erupting solitons in dissipative systems. Phys. Rev. Lett. **85**, 2937 (2000)
90. Soto-Crespo, J.M., Akhmediev, N., Mejia-Cortes, C., Devine, N.: Dissipative ring solitons with vorticity. Opt. Exp. **17**, 4236–4250 (2009)
91. Szameit, A., Burghoff, J., Pertsch, T., Nolte, S., Tünnermann, A., Lederer, F.: Two-dimensional soliton in cubic fs laser written waveguide arrays in fused silica. Opt. Exp. **14**, 6055–6062 (2006)
92. Thual, O., Fauve, S.: Localized structures generated by subcritical instabilities. J. Phys. **49**, 1829 (1988) (Paris)
93. Tlidi, M.: Three-dimensional crystals and localized structures in diffractive and dispersive nonlinear ring cavities. J. Opt. B: Quantum Semiclass. Opt. **2**, 438 (2000)
94. Tlidi, M., Haelterman, M., Mandel, P.: 3D patterns and pattern selection in optical bistability. Europhys. Lett. **42**, 505 (1998)
95. Tlidi, M., Mandel, P.: Three-dimensional optical crystals and localized structures in cavity second harmonic generation. Phys. Rev. Lett. **83**, 4995 (1999)
96. Tlidi, M., Vladimirov, A.G., Pieroux, D., Turaev, D.: Spontaneous motion of cavity solitons induced by a delayed feedback. Phys. Rev. Lett. **103**, 103904 (2009)
97. Ultanir, E.A., Stegeman, G., Michaelis, D., Lange, C.H., Lederer, F.: Stable dissipative solitons in semiconductor optical amplifiers. Phys. Rev. Lett. **90**, 253903 (2003)
98. van Saarloos, W., Hohenberg, P.C.: Pulses and fronts in the complex Ginzburg-Landau equation near a subcritical bifurcation. Phys. Rev. Lett. **64**(7), 749–752 (1990)
99. Veretenov, N., Tlidi, M.: Dissipative light bullets in an optical parametric oscillator. Phys. Rev. A **80**, 023822 (2009)
100. Weiss, C.O., Larionova, Y.: Pattern formation in optical resonators. Rep. Progr. Phys. **70**, 255 (2007)

101. Yang, J.: Nonlinear Waves in Integrable and Nonintegrable Systems. SIAM, Philadelphia (2010)
102. Yang, J., Musslimani, Z.H.: Fundamental and vortex solitons in a two-dimensional optical lattice. Opt. Lett. **28**, 2094–2096 (2003)
103. Zezyulin, D.A., Alfimov, G.L., Konotop, V.V.: Nonlinear modes in a complex parabolic potential. Phys. Rev. A **81**, 013606 (2010)
104. Zhu, W., He, Y., Malomed, B.A., Mihalache, D.: Two-dimensional solitons and clusters in dissipative lattices. J. Opt. Soc. Am. B **31**, A1–A5 (2014)